THE ASTROPHYSICAL JOURNAL, 220:962–979, 1978 March 15

STELLAR MODEL CHROMOSPHERES. VII. CAPELLA (G5 III+), POLLUX (K0 III), AND ALDEBARAN (K5 III)

WALTER L. KELCH, JEFFREY L. LINSKY,*† AND GIBOR S. BASRI†
Joint Institute for Laboratory Astrophysics, University of Colorado and National Bureau of Standards
HONG-YEE CHIU†
Goddard Institute for Space Studies
SHENG-HUEI CHANG
Department of Physics, City College of the City University of New York
STEPHEN P. MARAN†
Laboratory for Astronomy and Solar Physics, NASA Goddard Space Flight Center
AND
INGEMAR FURENLID
Kitt Peak National Observatory‡
Received 1977 August 22: accepted 1977 September 16

ABSTRACT

Data from high-resolution SEC vidicon spectroscopy with a ground-based telescope (for the Ca II K line) and from spectral scans made with the BUSS ultraviolet balloon spectrograph (for the Mg II *h* and *k* lines) are used to derive models of the chromospheres and upper photospheres of three G–K giants. The models are based on partial redistribution analyses of the Ca II K line wings and cores and on the fluxes in the Mg II lines. The photospheres thus computed are hotter than predicted by radiative equilibrium models. T_{min}/T_{eff} is found to decrease with decreasing T_{eff}, while m_0 (the mass column density at the top of the chromosphere) increases with decreasing stellar surface gravity. The computed pressure at the chromosphere top in the primary member of the Capella spectroscopic binary system is 70 times smaller than the transition-region pressure derived by Haisch and Linsky, which suggests that additional terms must be included in the transition-region energy equations for giant stars. Estimates of the Ca II and hydrogen column densities are made for the circumstellar envelope of Aldebaran.

Subject headings: Ca II emission — stars: chromospheres — stars: emission-line — stars: late-type — ultraviolet: spectra

I. INTRODUCTION

Semiempirical upper photosphere and chromosphere models were proposed in earlier papers for the stars Procyon (α CMi, F5 IV–V; Ayres, Linsky, and Shine 1974, hereafter Paper II), Arcturus (α Boo, K2 IIIp; Ayres and Linsky 1975, Paper III), the Sun (G2 V; Ayres and Linsky 1976), and α Cen A and B (G2 V and K1 V; Ayres *et al.* 1976, hereafter Paper V). These models were constructed to match theoretical line profiles with observed Ca II K and Mg II *h* and *k* absolute flux profiles. The aim of this series of papers is to examine stars encompassing a wide range in spectral and luminosity class and to search for trends in the parameters that characterize the temperatures and densities of these atmospheric regions. Ultimately, we intend to compare the semiempirical results with models based on realistic theories of acoustic energy generation and dissipation.

This paper extends the analysis to three G and K giants. These stars were chosen because (1) they are a homogeneous group in the H-R diagram; (2) they are bright and hence readily observable at the K line; (3) calibrated observations of the Mg II *h* and *k* lines now exist; and (4) the stellar surface gravities and metallicities are reasonably well known.

Haisch and Linsky (1976) analyzed the ultraviolet emission spectrum of the spectroscopic binary Capella (α Aur). They concluded that the chromosphere-corona transition region of the primary star is similar to that of a solar plage (active region) with a transition-region (TR) pressure $P_{TR} \approx 10\,P_{\odot} \approx 1.5$ dyn cm^{-2}, whereas Mullan (1976) derived a coronal base pressure $P_{CB} \approx 0.016$ dyn cm^{-2} from scaling arguments. Assuming an energy equation that is valid for the solar TR, the Capella primary's TR is thin and P_{TR} is inconsistent both with P_{CB} and with the chromospheric pressure derived in the present analysis. We propose a possible resolution of this discrepancy.

* Staff Member, Quantum Physics Division, National Bureau of Standards.
† Visiting Astronomer, Kitt Peak National Observatory.
‡ Operated by the Association of Universities for Research in Astronomy, Inc., under contract with the National Science Foundation.

TABLE 1

STELLAR INFORMATION AND ESTIMATED T_{min} AND CHROMOSPHERIC PARAMETERS

Star	α Aur (G5 III+)	β Gem (K0 III)	α Tau (K5 III)
composition*	solar	solar	solar
T_{eff}* (K)	5280±200	4830±150	3800±200
log g* (cm s^{-2})	2.62±0.2	2.9±0.2	1.4±0.2
T_{min} (K)	4700	3805	2700
$m(T_{min})$ (gm cm^{-2})	1.0	0.3	0.3
T_{min}/T_{eff}	0.89	0.79	0.71
microturbulence† (km s^{-1})	2-10	2-10	2-10
log m_o (gm cm^{-2})	-4.25±0.35	-4.8±0.3	-3.85±0.3
P_o (dynes cm^{-2})	2.3(-2)	1.6(-2)	3.5(-3)
P_o^2/g	1.3(-6)	3.2(-7)	5.0(-7)

*see §II for references

†see §IIIa

We discuss our choice of fundamental parameters for these stars in § II, review our methods of analysis in § III, describe the observations and their absolute calibration in § IV, present the calculations and our proposed models in § V, compare these models with previous ones and discuss the implications for these and other stars in § VI, and conclude in § VII. This paper is a joint effort by several authors who contributed in different ways. The Ca II observations were made by Chiu, Linsky, Basri, and Maran and reduced by Chang and Basri. The spectrophotometry was performed by Furenlid and the final calibration by Kelch. Theoretical modeling was done by Kelch, and the paper was written by Kelch and Linsky.

II. STELLAR PARAMETERS

Although our methods for deriving atmospheric models are independent of effective temperature (see § III*a*), we estimate T_{eff} for the purpose of specifying radiative equilibrium models for comparison with our semiempirical models. The stellar surface gravity and metallicity, however, are necessary for the determination of the electron pressures and opacities in the semiempirical models. The stellar parameters discussed in this section are summarized in Table 1.

a) Surface Gravities

Wright (1954) obtained a mass of 3.03 $\mathfrak{M}_\odot$ and a radius of 14.1 $R_\odot$ for the α Aur primary, which give log g = 2.62. Although this radius has been generally adopted in subsequent work, it may be inaccurate owing to Wright's use of T_{eff} = 4650 K. Since the change in log g due to an increase in T_{eff} from 4650 K to our adopted value of 5280 K is 0.2 dex, we adopt log g = 2.62 ± 0.2.

Since β Gem (Pollux) is not a known binary, its mass has not been measured directly, nor is there in the literature a spectrosopically determined gravity for the star. Gustafsson, Kjaergaard, and Andersen (1974) estimated log g = 2.9, and Conti *et al.* (1967) estimated log g = 2.8, both from the $[g] \sim [L]^{-1}[M][T_{eff}]^4$ scaling relation where $[X]$ means $X/X_\odot$. We adopt log $g_{\beta\,Gem}$ = 2.9 ± 0.2 as the Gustafsson *et al.* mass follows from the $\mathfrak{M}(T_{eff}, M_{bol})$ relation of Iben (1967), whereas the Conti *et al.* mass is an estimate.

For α Tau (Aldebaran) there are several methods of deriving the gravity. First, Conti *et al.* (1967) derived, by scaling arguments, log g = 1.8, assuming $\mathfrak{M}_{\alpha\,Tau}$ = 5.0 $\mathfrak{M}_\odot$. However, Iben's (1967) and Paczyński's (1970) evolutionary tracks show that for $M_{bol} = -1.2 \pm 0.5$ ($M_V = -0.2$, BC = −1.0) and T_{eff} = 3700–3900 K, $\mathfrak{M} \lesssim 3\,\mathfrak{M}_\odot$. A reduction of the Conti *et al.* mass by a factor of 2 gives log g = 1.5. Second, one can directly compute the gravity from a measured angular diameter and parallax, given a mass. Using the angular diameter of Currie, Knapp, and Liewer (1974) of 0".024 and the Gliese (1969) parallax of 0".050 with $\mathfrak{M} \lesssim 3\,\mathfrak{M}_\odot$ as an upper limit, one finds log $g \lesssim$ 1.5. Third, van Paradijs and Meurs (1974) have done an LTE spectroscopic analysis of α Tau by using the ionization equilibrium of Fe I and found log g = 1.3 ± 0.35. However, Ramsey (1977*a*, *b*) has shown that departures from LTE ionization equilibrium can lead to low spectroscopic determinations of the gravity in late-type giants. It is useful to compare the gravity of α Tau with that of α Boo, which has been thoroughly studied (Ayres and Johnson 1977), and which has an accurate angular diameter and parallax. Ayres and Johnson find log $g_{\alpha\,Boo}$ = 1.6, and

from this, $\mathfrak{M}_{\alpha\,\mathrm{Boo}} = 1.1\ \mathfrak{M}_\odot$, given the calculated radius. From the similarly calculated radius of α Tau and an assumed mass of at most $\sim 3\ \mathfrak{M}_\odot$, one finds $\log g_{\alpha\,\mathrm{Tau}} \leq (\log g_{\alpha\,\mathrm{Boo}} - 0.09) \lesssim 1.5$. We therefore adopt $\log g_{\alpha\,\mathrm{Tau}} = 1.4 \pm 0.2$.

b) *Metallicities*

For all three stars we use the solar abundances of Ross and Aller (1976), except that we use the Mount and Linsky (1975) carbon abundance in computing electron pressures and background opacities. We use the solar Mg abundance of Ayres and Linsky (1976) of $\mathrm{Mg/H} = 3.89 \times 10^{-5}$ and the solar abundance of Ayres (1977) of $\mathrm{Ca/H} = 2.40 \times 10^{-6}$ for the line-formation calculations. Our basis for generally assuming solar abundances is the work of Wright (1954) for α Aur, Gustafsson, Kjaergaard, and Andersen (1974) and Conti *et al.* (1967) for β Gem, and van Paradijs and Meurs (1974) and Tomkin and Lambert (1974) for α Tau.

c) *Effective Temperatures*

For α Aur and β Gem we derive effective temperatures from broad-band colors in the absence of measured angular diameters or detailed model-atmosphere analyses. Linsky and Ayres (1978, hereafter Paper VI) show that the $(V - I)$-T_{eff} correlation based on the mean colors of Johnson (1966) exhibits small scatter (at most ~ 100 K) and is independent of luminosity. Using their correlation and the colors of Johnson *et al.* (1966), we find $T_{\mathrm{eff}} = 5280$ K for α Aur and $T_{\mathrm{eff}} = 4830$ K for β Gem. Effective temperatures determined from other colors are 5300 K (from $B - V$) and 5400 K ($I - L$) for α Aur, and 4790 K ($B - V$), 4810 K ($R - I$), and 4970 K ($I - L$) for β Gem. The α Aur value should be much closer to that of the primary than the secondary, since the primary is brighter in the visual by 0.25 mag (Wright 1954) and relatively even brighter in the near-infrared. We therefore adopt 5280 K for α Aur and 4830 K for β Gem. Owing to the similarity of the α Aur secondary to the primary (Wright [1954] estimated the spectral types as G5 III and G0 III and Morgan, Keenan, and Kellman [1943] assigned spectral types of G5 and F6), there is likely to be a significant contribution to the Ca II flux from the secondary. This is discussed in § IV*a*(iii).

Johnson (1966) reviewed previous estimates of the effective temperature of α Tau. He noted that the Pease (1931) angular diameter gives $T_{\mathrm{eff}} = 3860$ K, the $I - L$ color gives 3830 K, and a blackbody curve fit gives the 3600 K. Other colors (Johnson *et al.* 1966) yield the following values: 3780 K ($B - V$), 3660 K ($R - I$), and 3690 K ($V - I$). More recently, van Paradijs and Meurs (1974) found $T_{\mathrm{eff}}(\alpha\ \mathrm{Tau}) = 3970 \pm 70$ K relative to an α Boo value of 4350 K in their differential abundance analysis, and the angular diameter of Currie *et al.* gives $T_{\mathrm{eff}}(\alpha\ \mathrm{Tau}) = 3610$ K. Ramsey (1977*a*) has adopted a temperature of 3900 K. Owing to such a wide range of values, we adopt $T_{\mathrm{eff}}(\alpha\ \mathrm{Tau}) = 3800 \pm 200$ K.

III. COMPUTATIONAL PROCEDURES

a) *The Method*

Our basic approach has been described in previous papers of the series and will only be briefly summarized here. We start with an initial radiative equilibrium (RE) model computed for an assumed T_{eff} and $\log g$. We then modify the $T_e(m)$ structure (where m = mass column density in g cm^{-2}) of the upper photosphere to force agreement of our partial coherent scattering calculations with observations of the Ca II K wings. This also provides a preliminary value for T_{min}. For this analysis, we chose points in the wings which appeared relatively free of absorption lines or any known emission features (see Stencel 1977). For this $T_e(m)$ model we compute the electron pressures, assuming the metals are in LTE but solving the transfer–statistical equilibrium equations for a three-level-plus-continuum representation of hydrogen. We solve the transfer equations explicitly for the Lyman continuum and Hα, treat the Balmer and Paschen continua as fixed rates by using photospheric radiation temperatures interpolated among the Ayres (1975) values for the Sun, α Boo, and α Cen B, and assume detailed balance for Lα and Lβ, since they are formed outside our region of interest.

We next assume a chromospheric $T_e(m)$ distribution in which $T_e(m)$ increases linearly in $\log m$ from T_{min} to $T_0 = 8000$ K at m_0 ($\tau_{\mathrm{Ly\ cont}} \approx 1.0$). $T_e(m)$ then increases rapidly above m_0 to 20,000 K to simulate the beginning of a transition region and to rapidly ionize H (which forces $\tau_{\mathrm{Ly\ cont}} \approx 1$ at m_0) and Ca^+ and Mg^+ (which forces K, h, and k to form below m_0). For this $T_e(m)$ distribution, we derive P_e and solve the hydrogen statistical equilibrium equations as described above.

We next compute the Ca II K line core, assuming partial redistribution (PRD), and compare this line profile with the observations: (1) at K_1[1] to determine the structure near T_{min}, specifically the value of T_{min} and the mass column density $m(T_{\mathrm{min}})$ where the temperature minimum occurs; and (2) to match the integrated emission fluxes to determine the lower chromospheric structure and provide a crude estimate of m_0. Mg II h and k line profiles are then computed to test the assumed chromospheric structure up to m_0 by using the basic PRD method of Milkey and Mihalas (1973). Finally, by a trial-and-error procedure, we modify the chromospheric model to optimally fit the Ca II K profiles and the Ca II K and Mg II h and k integrated emission fluxes.

For the line profile calculations we use a microturbulence of 2 km s^{-1} in the photosphere which increases linearly with $\log m$ to 10 km s^{-1} at m_0 and is constant at 10 km s^{-1} above m_0. The value of 10 km s^{-1} at m_0 was found to fit best the Ca II resonance-line profiles of the Sun, α CMi, and α Cen A, and is midway between those found for α Boo and α Cen B. This value appears suitable for matching the K_2 emission feature of the stars studied here, but

[1] The mean of the minimum features $\mathrm{K}_{1\,\mathrm{blue}}$ and $\mathrm{K}_{1\,\mathrm{red}}$ on either side of the emission core.

changes in the turbulence at m_0 of up to a factor 2 alter the calculated integrated emission fluxes of the stars previously studied by less than 6% (Ayres 1975).

Our semiempirical method thus determines a plane-parallel, homogeneous, hydrostatic equilibrium model of the upper photosphere ($\tau_c \lesssim 0.3$) and chromosphere $m(T_{\min}) < m < m_0$, $T_{\min} < T < T_0$ and differs from theoretical models in that it determines a model without the constraint of radiative equilibrium.

b) Model Atoms and Atomic Data

i) Ca^+

We use a three-level-plus-continuum representation for Ca^+, including the $4s\ ^2S_{1/2}$ ground state (level 1), $4p\ ^2P_{3/2}$ excited state (level 3), $3d\ ^2D_{5/2}$ metastable level (level 2), and Ca^+ continuum ($Ca^{+\,+}$). We solve the transfer equations explicitly for Ca II K (1–3) and λ8542 (2–3), thus including cross-redistribution or fluorescence between the infrared triplet and the K line by using the approach of Milkey, Shine, and Mihalas (1975), but still avoiding the much greater computing effort required for a full five-level treatment (calculating H, K, and three infrared triplet lines). As discussed in Paper V, the differences in the K line profile between a five- and a three-level PRD calculation are minimal. Collisions couple all levels, and we include photoionizations from the three bound levels as fixed rates determined by the local temperatures in the photosphere and lower chromosphere and by radiation temperatures from the mid-chromosphere outward as suggested by Ayres (1975), interpolating linearly in $P_0(\equiv m_0 g)$ among his values for the Sun, α Boo, and α Cen B. We adopt the atomic parameters, collision rates, and photoionization cross sections of Shine and Linsky (1974) except for the van der Waals broadening constant γ_{VW}(K), for which we use 1.7×10^{-8} as found by Ayres (1977).

ii) Mg^+

We use a three-level-plus-continuum representation for Mg^+, including the $3s\ ^2S_{1/2}$ ground state (level 1), $4p\ ^2P_{1/2}$ and $4p\ ^2P_{3/2}$ excited states (levels 2 and 3, respectively), and the Mg^+ continuum ($Mg^{+\,+}$). We solve the transfer equations explicitly for Mg II h and k (1–2 and 1–3, respectively), and include collisions coupling all levels and the continuum and photoionizations from the three bound levels treated in the same manner as for Ca^+. We adopt the atomic parameters, collision rates, and photoionization cross sections of Shine (1973), except for $\gamma_{VW}(h$ and $k) = 1.0 \times 10^{-8}$ as found by Ayres and Linsky (1976).

IV. THE OBSERVATIONS AND THEIR CALIBRATION

a) Ca II K

i) *The Observations*

The Ca II K line observations were obtained with the McMath Solar Telescope at Kitt Peak National

TABLE 2

JOURNAL OF OBSERVATIONS

Star	Line	Date	Start time (MST)	Integration time(min)	Frame number	Air mass	Binary phase	Circumstellar velocity (km s^{-1})	Circumstellar equivalent widths (mA)	Circumstellar Ca II column density (cm^{-2})	Profile in figure
α Aur	K	10/27/76	0320	5	7610-3-1	1.0	0.47				1
	K	10/26/76	0014	16	7610-1-2	1.3	0.46				1
	K*	9/14/76	0502	29	7609-5-3	1.9	0.06				
	K	2/27/76	2312	15	7602-14-1	1.6	0.14				
	K	12/16/75	0101	30	7512-37-2	1.2	0.34				
	K	10/28/75	2215	30	7510-30-3	2.0	0.97				
	H*	9/17/76	0223	8	7609-14-4	1.2	0.09				
β Gem	K	9/16/76	0436	60	7609-11-4	1.1					1
	H	9/19/76	0451	61	7609-24-1	1.1					
α Tau	K	10/29/76	0005	60	7610-8-5	1.3		-30			1,2
	K	10/27/76	0446	40	7610-3-3	1.2		-28			2
	K*	9/16/76	0208	50	7609-11-2	1.3		-33			1,2
	K*	9/14/76	0246	120	7609-5-2	1.5		-30			2
	K	2/28/76	0237	50	7602-21-3	1.4		-21			2
	K	2/26/76	2143	40	7602-8-2	1.0		-22			2
	H	10/29/76	0136	60	7610-9-3	1.1			14.2	3.1×10^{11}	3
	H**	9/17/76	0237	50	7609-14-5	1.5			16.9	3.7×10^{11}	3

*Close in time to BUSS observations of de Jager et al. (1976).

**Simultaneous with BUSS observations.

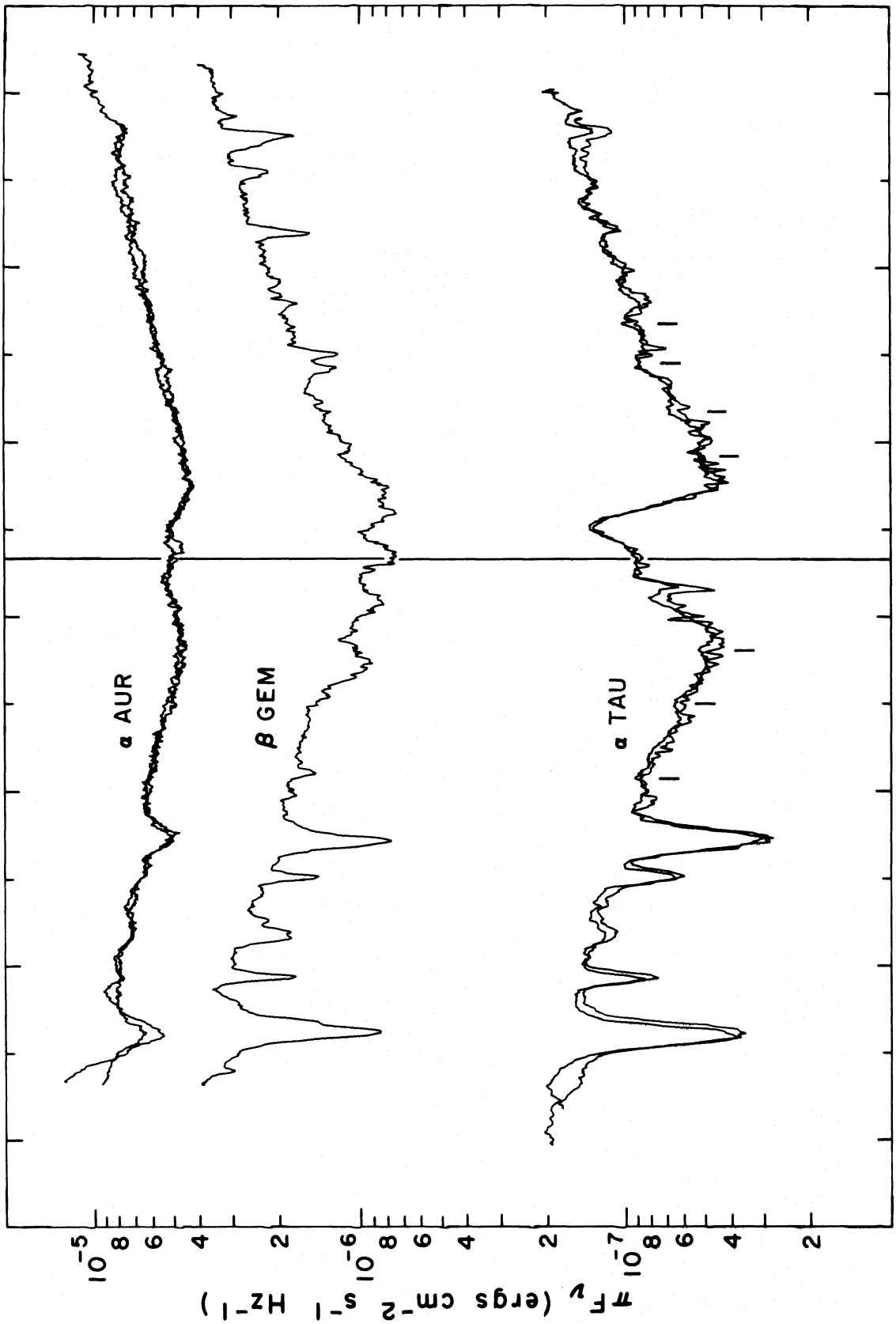

FIG. 1.—Absolute flux spectra obtained with an integrating SEC vidicon camera and a 2 m echellette spectrograph with the McMath Solar Telescope at Kitt Peak National Observatory. The spectral resolution is 55 mÅ, and the wavelength scale is corrected for stellar and heliocentric radial velocities. *Vertical bars*, emission or absorption lines given in Table 3. Circumstances of the observations are given in Table 2.

Observatory, using a new 2 m Czerny-Turner spectrograph developed by Dr. D. M. Hunten. The 128 mm square echellette grating, ruled with 316 lines mm^{-1}, was used in the 15th order for this work. Detection and recording were accomplished with the integrating SEC vidicon camera system developed by Chiu (1977). Further details of the instrumentation and data processing techniques are presented in Chiu *et al.* (1977), which describes earlier results obtained with the main 13.7 m vertical spectrograph. In the present work, the Hunten spectrograph was mounted in the FTS observing room of the telescope building. As it has a better grating and is faster, the 2 m spectrograph provided much shorter exposure times than we attained on the same stars with the vertical spectrograph, at a slight sacrifice of spectral resolution. Also, telescope time is used more efficiently in the present configuration, and less hazard is presented to the vidicon system, since it is unnecessary to remove the vidicon from the spectrograph each morning in order to permit other observers to study the Sun.

Useful observations of the Ca II K profiles of Capella, Pollux, and Aldebaran were obtained on several occasions, as summarized in Table 2. Each observation (vidicon frame) records about 12 Å of the spectrum, centered on Ca II K or H. The profiles actually analyzed in the present paper are illustrated in Figure 1. We have acquired a number of spectra of Pollux, but list only the best set in Table 2, as the K line does not show any detectable variability at our spectral resolution. We conclude that this star is inactive, as previously noted by Liller (1968). Capella also shows no important variations except for Doppler shifts of the primary star, which we discuss below in § IV*a*(iii). Aldebaran, however, is a very active star (see Liller 1968), and we comment on its circumstellar shell in § VI*a*(iii).

The 1976 September Ca II H and K observations of Capella and Aldebaran, in addition to other stars, were obtained simultaneously or near-simultaneously with SEC vidicon echelle spectroscopy performed by the upgraded BUSS payload of de Jager *et al.* (1976). In a subsequent publication we will compare these Mg II high-resolution profiles with the simultaneous Ca II profiles.

Each spectrum in Figure 1 shows emission near K line center and broad absorption in the K line wings. In addition, there are many absorption lines due to iron and other metals, and, especially in α Tau, emission features due to rare-earth and iron group lines (see Stencel 1977). A summary of the emission lines seen in the wings of H and K is given in Table 3 and the location of these lines is noted in Figures 1 to 3. There are several points to note in the Ca II data. First, the α Aur K wing absorption is shallow and the K emission and other absorption-line features are washed out. This appearance of the spectrum is presumably due to the presence of a hotter rapidly rotating secondary (see Herbig and Spalding 1955). Second, β Gem appears to have three emission features. Actually, the bluest feature is not due to Ca II but rather to absorption at λ3932.3 and perhaps also

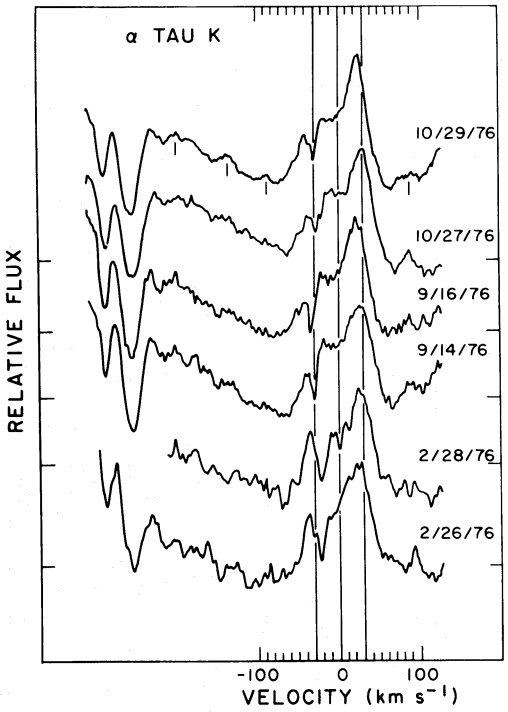

FIG. 2.—Alpha Tau K line profiles on six occasions during 1976. Major circumstellar absorption features occur at −21 to −33 km s^{-1}, and additional features at +1 and +4 km s^{-1} in the 1976 February 28 profile and adjacent to the major CS profiles in other profiles may also be present. *Vertical bars*, emission lines given in Table 3. *Ticks on vertical axis*, zero relative flux for each successive line profile.

to Fe I emission at λ3932.7 (Stencel 1977). Third, the central intensities of the strong absorption features at λ3928 and λ3930.3 are as deep or deeper than K_1 for β Gem and α Tau. These two features are resonance lines of the fourth multiplet of Fe I and are most likely formed almost entirely by scattering. The narrow absorption at λ3933.3 in α Tau will be discussed in § VI*a*(iii).

ii) *Calibration*

The conversion to absolute flux at the top of the atmosphere involved two steps. First, the vidicon data were calibrated by 1 Å bandpass (FWHM Gaussian) spectrophotometry of the three stars in the range λλ3850–4050. Plates were taken with the coudé spectrograph of the 2.1 m KPNO telescope, using the 0.9 m coudé feed as the light collector. A wide slit, around 10″, was used to ensure that true fluxes were observed. In each case, the program star and Vega or a secondary standard together with wavelength-dependent calibration were exposed on the same plate, matching the densities as closely as possible. This method involves only relative photometry to the standard star and corrections for atmospheric transmission. We then smoothed the vidicon spectra by the 1 Å Gaussian coudé instrumental profile for comparison with the coudé spectrophotometry. This comparison for β Gem and α Tau showed that the deeper

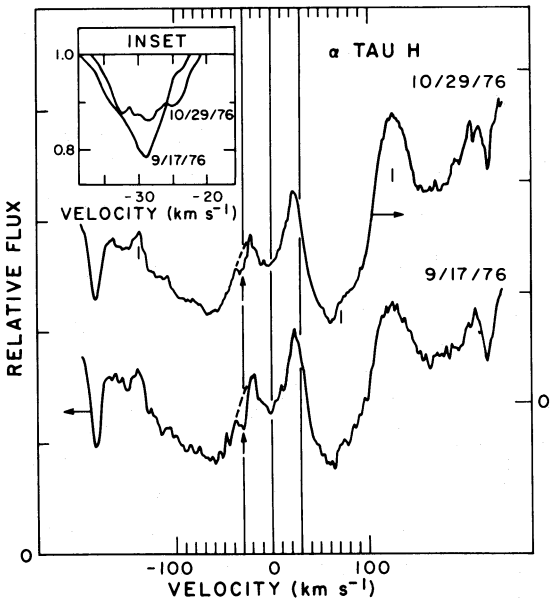

FIG. 3.—Alpha Tau H line profiles. *Vertical arrows*, velocities corresponding to CS absorption features in the K line profiles obtained at about the same time. *Horizontal arrows*, relative flux axis for each profile. *Dashed lines*, estimated H line profiles for no CS absorption. *Vertical bars*, emission lines given in Table 3. The inset gives CS line profiles in residual intensity units, obtained by taking the ratio of the observed to the estimated intrinsic H line profiles.

inner wings on either side of the K line emission are relatively brighter in the spectrophotometry than in the smoothed vidicon spectra, perhaps owing to scattered light in the coudé spectrograph. To estimate this scattered light by means of computer experiment, we added intensity equivalent to white scattered light to the smoothed vidicon data sufficient to match the spectrophotometry, namely, 0.25% of the 4000 Å continuum for β Gem and 0.35% for α Tau. We then calibrated the vidicon spectra by using a linear interpolation between the calibration factors established at 1 Å intervals.

Models derived by using this calibration and reported by Kelch *et al.* (1976) appeared unrealistically hot and suggested a systematic calibration error. As a second step in our calibration, we therefore recalibrated the 1 Å bandpass α Tau spectrophotometry by the 25 Å bandpass spectrophotometry of Honeycutt *et al.* (1977). We found a discrepancy which appeared to be independent of wavelength over the range $\lambda\lambda$3910–3990. We then reduced the α Tau data by a factor of 1.94 to match the Honeycutt *et al.* absolute calibration. Since no other relevant spectrophotometry of α Aur or β Gem is in the literature, we applied the same recalibration factor to our data for these stars. As a consistency check, we compared 1 Å spectrophotometry over a 200 Å range to the narrow-band "40" filter magnitudes of Johnson (1967) for the three stars, and found the magnitude differences between α Tau and the other two stars to be the same as the corresponding Johnson magnitude differences to within 10%. We estimate the overall accuracy of the above calibrations to be $\pm$15%–20%.

To convert the absolute fluxes to stellar surface fluxes (ergs cm^{-2} s^{-1} Hz^{-1}), we estimated angular diameters by using the $V - R$ formula of Barnes and Evans (1976) and the colors of Johnson (1967). The measured angular diameter of α Tau (Currie *et al.*) is 0".024 and the Barnes and Evans (1976) calculated

TABLE 3

EMISSION LINES NOTED IN THE WINGS OF H AND K

λ	α Aur	β Gem	α Tau	Preliminary ID*
3931.1	N	A	E	Fe I 565
3932.0	N	E?	E	Ti II 34
3932.7	N	E?	E	Fe I 380, 562
3934.8	N	E	E	Nd II or Zr II 43
3935.3	N	N	E	Fe I 362
3935.9	N	A	E	Fe I 362, 564 and Fe II 173
3936.22	N	N	E?	La II 13
3964.75	E	N	E?	He I 5
3966.6	N	N	E	Fe I 562, 282
3969.4	N	N	E?	Fe II 3
3970.07	N	N	E	Hε

*From Stencel (1977).

E = emission, A = absorption, N = no line seen

TABLE 4

INTEGRATED EMISSION FLUXES (ergs cm^{-2} s^{-1})

	Star/model	Ca II K (bandpass, Å)	Mg II h + k (k/h bandpasses, Å)	k/h
	α Aur	1.56±0.4(+6) (±0.90)	3.6±1.1(+6)* (±2.5/±1.6)	1.43*
A	4700/5700/8000 0.0/-1.8/-4.0	1.66(+6) (±0.90)	3.52(+6) (±1.94/±1.6)	1.21
B	4700/5700/8000 0.0/-1.8/-4.5	1.56(+6) (±0.90)	2.85(+6) (±1.94/±1.6)	1.19
	β Gem	1.98±0.3(+5) (±0.55)	3.5±1.0(+5)* (±1.5/±1.0)	1.38*
A	3805/4900/8000 -0.52/-2.2/-4.8	2.00(+5) (±0.55)	3.57(+5) (±1.35/±1.1)	1.19
B	3805/4800/8000 -0.52/-2.2/-4.7	1.72(+5) (±0.55)	3.51(+5) (±1.35/±1.1)	1.20
C	3805/5000/8000 -0.52/-2.5/-4.7	1.58(+5) (±0.55)	2.66(+5) (±1.3/±1.1)	1.18
D	3805/5000/8000 -0.52/-2.5/-5.0	1.62(+5) (±0.55)	1.94(+5) (±1.25/±1.1)	1.16
E	3780/8000 -0.52/-4.5	8.85(+5) (±0.79)	--- ---	---
	α Tau	2.9±0.5(+4) (±0.90)	6.7±2.0(+4)† (±1.25/±1.4)	1.28†
A	2700/5000/8000 -0.52/-2.2/-4.1	3.10(+4) (±0.90)	5.07(+4) (±1.94/±1.5)	1.22
B	2700/5000/8000 -0.52/-2.2/-4.0	--- ---	5.66(+4) (±1.94/±1.5)	1.22
C	2700/8000 -0.46/-4.5	2.99(+4) (±0.90)	3.05(+4) (±1.94/±1.46)	1.21
D	2825/8000 -0.74/-5.66	1.5(+4) (±0.75)	--- ---	---
E	2825/8000 -0.22/-5.66	3.71(+4) (±1.1)	--- ---	---

*Kondo, Morgan and Modisette (1976).

†Kondo, Morgan and Modisette (1975).

value is 0".0235, in excellent agreement. The Barnes and Evans value for the α Aur primary is 0".0072, whereas a preliminary value (Blazit *et al.* 1977), using two-telescope interferometry and assuming no limb darkening, is 0".0052 ± 0".001. We adopt the Barnes and Evans value because of the preliminary nature of the observed value, and because there is little scatter to the Barnes and Evans relation at the α Aur color. The calibrated Ca II K line profiles are presented in Figure 1, and the integrated fluxes from $K_{1\,red}$ to $K_{1\,blue}$ are given in Table 4 together with the $K_{1\,red}$–$K_{1\,blue}$ bandpasses.

iii) *The Binary Nature of α Aurigae*

We consider now the possible contribution of the hotter (G0 III?) secondary star in the α Aur system to the observed K core and inner wing flux. Assuming a primary/secondary flux ratio of 1.25 at λ5500 (Wright 1954) and effective temperatures of 5280 K for the primary and 6000 K for the secondary, we estimate equal fluxes from the two stars at λ3934, assuming similar K line residual intensities. It is quite likely, therefore, that *about one-half* of the flux in the K core and inner wings is due to the secondary star. Herbig and Spalding (1955) estimated the rotation of the secondary to be $v \sin i \approx 85$ km s^{-1} from the appearance of the secondary's spectral lines. This rotation is sufficient to wash out the K emission of the secondary such that $K_2/K_1 \approx 1.0$ from the secondary. (Rotation in the other stars is negligible for our analysis.) Wright (1954) found that the K emission tended to follow the primary in radial velocity, and in a check of the vidicon data at phases of 0.14, 0.34, and 0.46, and 0.97 (see Table 2), we find that the K_2 emission definitely follows the primary.

The observed *h* and *k* emission fluxes, by orbital radial-velocity arguments, also appear to arise from the primary (Kondo *et al.* 1976). It is possible that the Capella *h* and *k* emission fluxes may include contributions from the secondary star, as is the case for Ca II K, especially as the secondary is hotter than the primary. However, the profiles of the secondary should have low h_2/h_1 and k_2/k_1 ratios owing to rapid rotation. Since the observed ratios are large (~5 in the Kondo, Morgan, and Modisette 1976 data), we conclude that,

although the secondary star may not be a major contributor to the observed Capella Mg II flux, the observed flux must be considered a maximum possible flux from the primary.

Although the Ca II K observations cannot be used to model accurately the upper photosphere of the α Aur primary, we can still estimate the K_1 flux and the integrated Ca II K emission flux. Assuming that the secondary's K flux is equal to the primary's and $K_2/K_1 = 1.0$ for the secondary, we subtract the secondary's flux from the observed flux to produce the calibrated spectrum seen in Figure 1. The K emission flux listed in Table 4 for the α Aur primary thus has a greater uncertainty than that for the other two stars, but is still of use for modeling the chromospheric structure.

b) Mg II *h and k*

The Mg II *h* and *k* line fluxes are obtained from the balloon-borne ultraviolet stellar spectrometer (BUSS) observations of Kondo, Morgan, and Modisette (1975, Fig. 1; 1976, Figs. 1, 2). Since the spectral resolution is 0.40 Å and the apparent noise level of the data is considerable, we use only integrated line core emission rather than the profiles in the subsequent analysis. To obtain the absolute integrated emission fluxes given in Table 4, we planimetered the profiles above zero signal from $k_{1\,\mathrm{red}}$ to $k_{1\,\mathrm{blue}}$ and from $h_{1\,\mathrm{red}}$ to $h_{1\,\mathrm{blue}}$ and converted to absolute units by using the conversion table (Table 1) of Kondo, Morgan, and Modisette (1976), which the authors estimate to be accurate to ±30%. As discussed in Paper VI, the integrated flux between the h_1 and k_1 features and above zero flux rather than above the h_1 and k_1 flux levels is an accurate measure of chromospheric emission in the Mg II lines. The conversion to stellar surface fluxes (ergs $\mathrm{cm}^{-2}\ \mathrm{s}^{-1}$) is as described above.

Copernicus observations of the Mg II lines (McClintock *et al.* 1975; McClintock 1977) give fluxes for α Tau and β Gem which are about a factor of 2 smaller than the BUSS data. The main reason for the apparent discrepancy is that it is difficult to correct for the particle background in the *Copernicus* data, and hence the dark level is hard to determine. Instead, the zero line is drawn through spectral regions of minimum flux, which, as the BUSS data show, actually contain substantial flux.

V. RESULTS

a) The Upper Photospheric Models

In Figure 4 we compare our semiempirical temperature distributions for α Aur, β Gem, and α Tau with LTE RE models. Kurucz (1977) provided us with models (see Kurucz 1974) computed with the gravities and effective temperatures of § II, except for T_{eff}(α Tau) = 3690 K. These models include statistically the effects of atomic but not molecular line blanketing. Thus the upper photosphere portions of these models, especially α Tau, may be too warm owing to the lack of molecular line cooling. The Bell *et al.* (1976) model is an

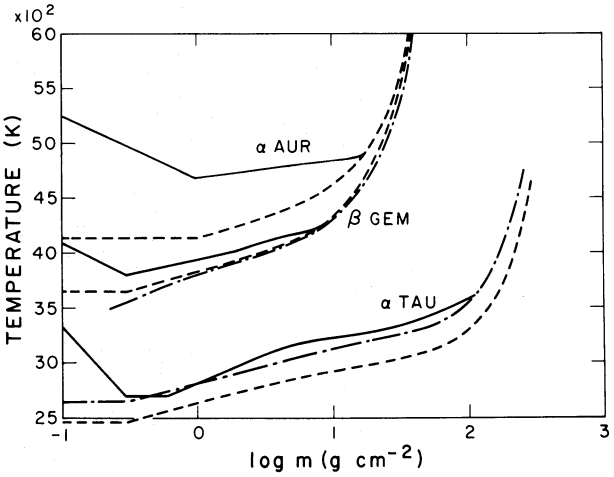

FIG. 4.—Model atmospheres. *Solid line*, semiempirical models; *dashed line*, Kurucz models; *dot-dashed lines*, Bell model for β Gem and Johnson model for α Tau. See § V*a* for details.

opacity distribution function (ODF) model for T_{eff} = 5000 K, log *g* = 3.0 scaled to T_{eff} = 4830 K, log *g* = 2.9. The Johnson (1973) model for α Tau is an opacity sampling (OS) model for T_{eff} = 3900 K, log *g* = 1.4 (scaled from log *g* = 1.6) which includes both atomic and molecular line opacities (see Johnson and Krupp 1976). All these models assume solar abundances. We incorporate the Johnson rather than the Kurucz model for the deep photosphere portion of our α Tau model, since it more closely matches the observed K line wing. The semiempirical α Aur primary upper photosphere model we use is merely a straight line in log *m* from the 4900 K level to T_{min} = 4700 K, determined from PRD core calculations.

Figure 5 shows computed K line wings for each of the various β Gem and α Aur models of Figure 4 except the Bell *et al.* β Gem model, which predicts essentially the same wing as the Kurucz β Gem model. Also shown are the observed wing fluxes, and the effects on the wing calculations of ±50 K changes in the models. We find that the RE models predict K line wings which are darker than observed, and are thus too cool in their upper photospheres. Also shown in Figure 5 are wing calculations for our proposed models without chromospheric rises in temperature [$dT/dm = 0$ for $m < m(T_{\mathrm{min}})$]. In previous papers we have estimated T_{min} by matching observations with the K wing calculations based on such models without chromospheres. This procedure is accurate for β Gem, as can be seen by comparing the computed wings in Figure 5 with the full PRD calculations in Figure 6. However, we find that matching the α Tau full PRD calculation at K_1 requires a steep upper photospheric temperature gradient, and the partial coherent scattering wing calculation without a chromosphere falls well below the observations at K_1. In the case of α Tau we therefore use the PRD calculations to determine T_{min}.

Ramsey (1977*a*) has derived a semiempirical model for α Tau based on an LTE analysis of the central

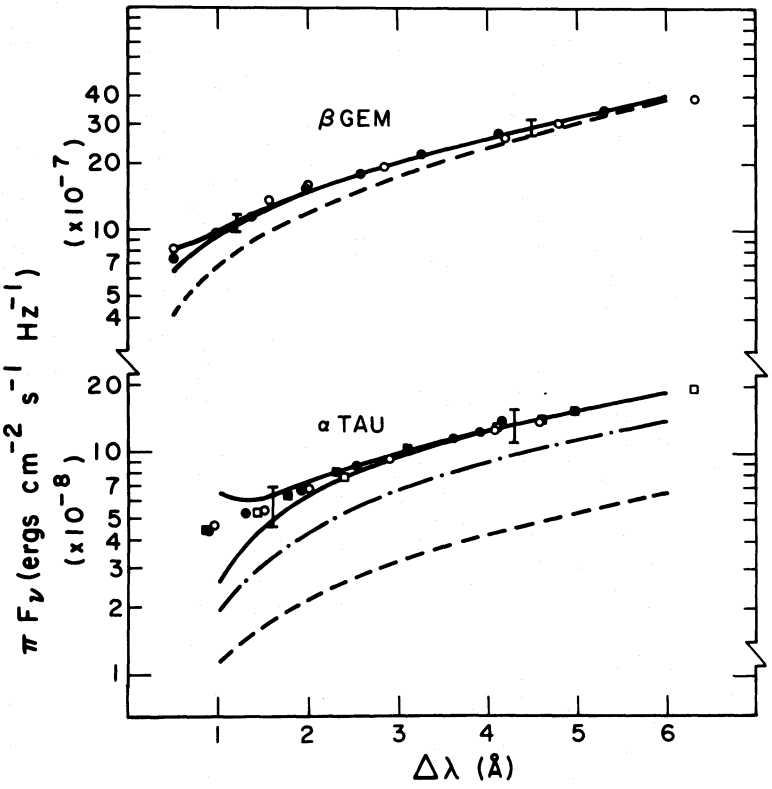

FIG. 5.—Observed and computed Ca II K wings. Model notations are the same as in Fig. 4, except that the lower solid curve for each star is the predicted wing flux for our semiempirical models without chromospheric rises in temperature. Error bars designate the effect of ±50 K changes in the models. We have one frame of data for β Gem and two frames for α Tau with the following symbols: *filled circles*, first frame, red (with respect to line center); *unfilled circles*, first frame, blue; *solid square*, second frame, red; *open circles*, second frame, blue.

intensities of Fe I lines in four multiplets, but his model departs significantly from Johnson's OS model for α Tau, as seen in Ramsey's Figure 2. Our proposed α Tau model agrees approximately with Ramsey's model at $\log m \approx 1.2$ and at the surface, but contrasts quite sharply elsewhere. We are not concerned about this discrepancy because Athay and Lites (1972) have shown for the Sun that the source functions of Fe I lines originating from metastable levels fall below the local Planck function, and Ramsey's model for α Tau is determined solely by such lines at $\log m \lesssim 1.0$. Ramsey noted this as well as the possibility that the source functions of the Fe I lines are photoionization-dominated and therefore tend toward J_ν rather than B_ν at all depths.

b) The Chromospheric Models

Table 4 summarizes observed and computed integrated emission fluxes of Ca II K and Mg II *h* and *k* for various chromospheric models. The models are designated by letters and are generally ordered according to decreasing match to the observations. The notation is

$$\log m(T_{\min})\Big/^{T_{\min}}\ \log m_{\text{hinge}}\Big/^{T_{\text{hinge}}}\ \log m_0\Big/^{T_0}\ .$$

To match the Ca II K and Mg II *h* and *k* emission fluxes, we found it necessary, especially for α Tau and β Gem, to divide the chromosphere into two separate linear segments about a "hinge point." This gives the upper chromosphere a steeper temperature gradient, and is the simplest means of producing a $T(m)$ structure which is concave upward. Generally, we have chosen m_{hinge} such that K_2 is formed at or below m_{hinge} and the structure above m_{hinge} (determined by the value of m_0) has only a small effect on the K_2 flux.

Before we proceed, one datum of Table 4 requires explanation. The observations of the α Tau K line core as seen in Figure 1 show a sharp absorption feature blueshifted by about 30 km s^{-1}, probably owing to a variable circumstellar shell. We have therefore added back the flux needed to fill in the absorption but not produce a blue emission peak, as the Mg II *h* and *k* emission features (see Kondo, Morgan, and Modisette 1975, Fig. 1) as well as the Ca II H emission features (see Fig. 3) are also asymmetric. This increases the K integrated emission flux by only 3% to 7% for each frame, well within our calibrated uncertainty of 15%–20%.

The effect of changes in the various structural parameters are exhibited in Table 4 and Figure 6. The α Tau computations exhibit our search for $m(T_{\min})$. Note from

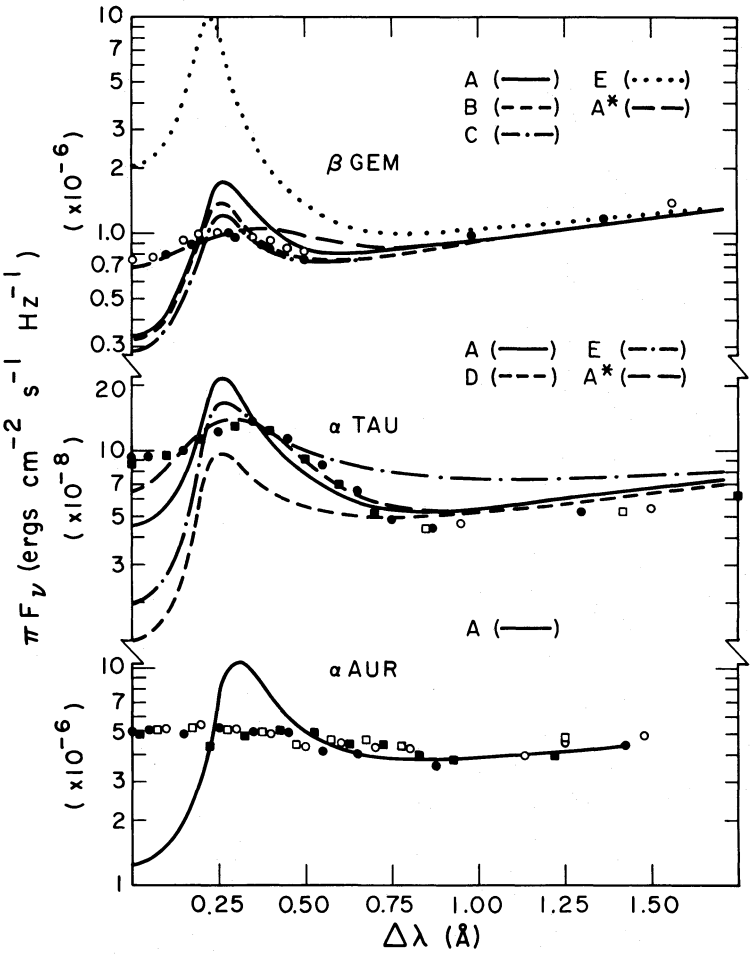

FIG. 6.—Comparison of PRD computed K line cores with observations. Data notation is the same as in Fig. 4. For explanation of the models, see Table 4 and § V*b*. Curves labeled *A** are models A convolved with a 20 km s^{-1} Gaussian for α Tau and a 30 km s^{-1} Gaussian for β Gem.

models D and E the sensitivity of K_1 to only a 0.5 dex change in $m(T_{min})$. One can understand this by considering the profile to be a mapping of the $T(m)$ structure. Because $m(T_{min})$ for model E is larger than for model D, each mass point in the lower chromosphere is hotter in model E, producing greater K emission. The unique sensitivity of the location of K_1 to $m(T_{min})$ is due to K_1's forming in the damping wing of the line rather than in the Doppler core, and thus not being sensitive to turbulent velocities. Clearly, the determination of $m(T_{min})$ is insensitive to errors in the flux scale. The α Tau model (model B) which best matches the Ca II and Mg II data is tabulated in Table 5.

The calculations shown in Figure 6 for the various β Gem models demonstrate changes in the K profile owing to the inclusion of and location of a hinge point in the chromosphere. Model E has no hinge point and results in too much K flux. A one-segment chromosphere with the proper temperature gradient to accurately predict the K emission flux would have $\log m_0$ of -6.5 to -7.0, and would predict far too little Mg II *h* and *k* emission. Model C has the same lower chromosphere temperature gradient as model B except that m_{hinge} is extended farther out by a factor of 2 in mass, decreasing the Mg II fluxes. The effect of increasing T_{hinge} by 100 K while keeping m_{hinge} constant is shown by the increase in K flux from model B to model A, while the Mg II fluxes are little changed owing to a slight decrease in m_0. Finally, the larger effect of changes in m_0 on the *h* and *k* emission fluxes compared with the K emission fluxes can be seen by comparing the predicted fluxes for α Aur models A and B, β Gem models C and D, and α Tau models A and C, pairs of models with the same lower chromospheric temperature gradients. The best-fit β Gem model is tabulated in Table 6.

The K profiles in Figure 6 exhibit larger K_2/K_3 ratios than are observed. Four effects which tend to decrease this ratio without changing the integrated K emission flux are rotation, macroturbulence, instrumental resolution, and (possibly) intermediate-scale

TABLE 5

α TAURI (MODEL B)

τ_c(5000Å)	m(g cm^{-2})	T_e(K)	P_e(dynes cm^{-2})	n_H(cm^{-3})	b_1(HI)
1.49(-05)	9.00(-05)	20000	7.56(-04)	3.40(+05)	1.22(+07)
1.66(-05)	9.50(-05)	12000	7.20(-04)	9.75(+06)	3.36(+05)
1.74(-05)	9.74(-05)	10000	6.95(-04)	2.53(+07)	3.55(+04)
1.80(-05)	1.00(-04)	8000	6.63(-04)	8.59(+07)	4.20(+03)
2.24(-05)	1.21(-04)	7866	7.10(-04)	3.32(+08)	2.51(+03)
3.38(-05)	1.85(-04)	7554	8.10(-04)	8.56(+08)	1.88(+03)
4.58(-05)	2.83(-04)	7242	8.37(-04)	1.94(+09)	1.40(+03)
5.69(-05)	4.32(-04)	6930	7.91(-04)	3.93(+09)	1.02(+03)
6.65(-05)	6.60(-04)	6618	6.95(-04)	7.38(+09)	7.30(+02)
7.42(-05)	1.00(-03)	6306	5.77(-04)	1.29(+10)	4.87(+02)
8.04(-05)	1.54(-03)	5994	4.78(-04)	2.30(+10)	2.92(+02)
8.50(-05)	2.35(-03)	5682	3.77(-04)	3.86(+10)	1.58(+02)
8.86(-05)	3.59(-03)	5370	2.92(-04)	6.82(+10)	7.88(+01)
9.11(-05)	5.49(-03)	5060	2.16(-04)	1.22(+11)	3.71(+01)
9.28(-05)	8.39(-03)	4801	1.61(-04)	2.03(+11)	2.01(+01)
9.40(-05)	1.28(-02)	4551	1.16(-04)	3.38(+11)	1.28(+01)
9.49(-05)	1.95(-02)	4301	8.59(-05)	5.64(+11)	8.85(+00)
9.56(-05)	2.99(-02)	4051	7.76(-05)	9.48(+11)	6.49(+00)
9.65(-05)	4.57(-02)	3800	1.02(-04)	1.60(+12)	4.55(+00)
9.80(-05)	6.98(-02)	3550	1.50(-04)	2.72(+12)	2.44(+00)
1.00(-04)	1.06(-01)	3300	1.73(-04)	4.69(+12)	1.04(+00)
1.05(-04)	1.62(-01)	3050	1.33(-04)	8.26(+12)	3.72(-01)
1.09(-04)	2.49(-01)	2800	7.00(-05)	1.59(+13)	1.12(-01)
1.12(-04)	3.00(-01)	2700	5.77(-05)	2.20(+13)	6.54(-02)
1.18(-04)	4.24(-01)	2700	7.54(-05)	3.17(+13)	6.43(-02)
1.28(-04)	6.00(-01)	2700	9.91(-05)	4.58(+13)	6.35(-02)
1.41(-04)	7.60(-01)	2750	1.36(-04)	5.58(+13)	8.32(-02)
1.59(-04)	9.50(-01)	2800	1.86(-04)	6.70(+13)	1.08(-01)
2.32(-04)	1.48(+00)	2900	3.52(-04)	9.67(+13)	1.79(-01)
4.36(-04)	2.38(+00)	3020	7.34(-04)	1.43(+14)	3.18(-01)
9.32(-04)	3.73(+00)	3110	1.35(-03)	2.13(+14)	4.76(-01)
2.04(-03)	5.73(+00)	3175	2.23(-03)	3.18(+14)	6.23(-01)
4.40(-03)	8.68(+00)	3220	3.40(-03)	4.75(+14)	7.14(-01)
9.18(-03)	1.30(+01)	3255	4.95(-03)	7.07(+14)	8.06(-01)
1.86(-02)	1.93(+01)	3285	7.05(-03)	1.04(+15)	8.91(-01)
3.66(-02)	2.82(+01)	3325	1.02(-02)	1.50(+15)	9.80(-01)
7.17(-02)	4.09(+01)	3375	1.52(-02)	2.15(+15)	1.08(+00)
1.32(-01)	5.90(+01)	3450	1.84(-02)	3.07(+15)	1.06(+00)
2.40(-01)	8.36(+01)	3530	3.10(-02)	4.20(+15)	1.05(+00)
4.54(-01)	1.14(+02)	3611	5.78(-02)	5.56(+15)	1.04(+00)

turbulence (Shine 1975). Radiative transfer among inhomogeneities may also produce such an effect (Owocki 1977). To approximately simulate these effects, we have convolved model A for α Tau and β Gem with Gaussian profiles of 20 km s^{-1} and 30 km s^{-1} FWHM respectively (see Fig. 6), which reasonably match the observations.

Table 7 summarizes our proposed parameters for the three stars. The value of $\log m_0(\alpha\ \mathrm{Tau}) = -3.85$ results from a small extrapolation of the results of α Tau models, A, B, and C. We estimate $\log m_0(\alpha\ \mathrm{Aur}) = -4.25$ because, as stated in § IV*a*(iii), the observed Mg flux may contain a contribution from the secondary and is therefore a maximum value for the primary. We do not wish to imply that our parameters are unique in the sense that the Ca II and Mg II data cannot be matched as well by a slightly different set or that the stellar chromospheres consist of only one component as assumed. We do feel, however, that the spatially averaged chromosphere of each star is reasonably matched by our set of parameters.

VI. DISCUSSION

a) Possible Sources of Error

i) *Data Calibration and Atomic Parameters*

The cited uncertainties in our measured line fluxes are ±15%–20% for K and ±30% for *h* and *k* (Kondo, Morgan, and Modisette 1976). In addition, these data must be converted to stellar surface fluxes with an additional uncertainty of ±20% due to a ±10% uncertainty in the angular diameters.

TABLE 6

β GEMINORUM (MODEL A)

τ_c(5000Å)	m(g cm $^{-2}$)	T_e(K)	P_e(dynes cm^{-2})	n_H(cm^{-3})	b_1(HI)
2.33(-06)	1.40(-05)	20000	5.42(-03)	2.50(+06)	1.75(+06)
2.49(-06)	1.45(-05)	12000	5.19(-03)	9.59(+07)	6.35(+04)
2.72(-06)	1.52(-05)	10000	5.03(-03)	2.33(+08)	6.08(+03)
2.85(-06)	1.58(-05)	8000	4.71(-03)	5.06(+08)	1.29(+03)
3.58(-06)	2.00(-05)	7881	4.71(-03)	1.50(+09)	4.29(+02)
6.01(-06)	3.31(-05)	7619	6.64(-03)	4.51(+09)	2.24(+02)
9.16(-06)	5.50(-05)	7359	7.91(-03)	1.27(+10)	1.54(+02)
1.27(-05)	9.13(-05)	7098	9.12(-03)	2.94(+10)	1.07(+02)
1.63(-05)	1.51(-04)	6837	9.55(-03)	6.03(+10)	7.56(+01)
1.99(-05)	2.51(-04)	6576	9.28(-03)	1.12(+11)	5.25(+01)
2.34(-05)	4.17(-04)	6315	8.45(-03)	1.98(+11)	3.59(+01)
2.65(-05)	6.92(-04)	6054	7.28(-03)	3.33(+11)	2.41(+01)
2.94(-05)	1.14(-03)	5793	5.96(-03)	5.45(+11)	1.57(+01)
3.20(-05)	1.90(-03)	5532	4.64(-03)	8.74(+11)	9.99(+00)
3.42(-05)	3.16(-03)	5271	3.44(-03)	1.38(+12)	6.21(+00)
3.60(-05)	5.25(-03)	5010	2.43(-03)	2.21(+12)	3.81(+00)
3.76(-05)	8.71(-03)	4814	1.91(-03)	4.42(+12)	3.69(+00)
3.90(-05)	1.44(-02)	4670	2.01(-03)	9.06(+12)	2.95(+00)
4.11(-05)	2.40(-02)	4526	2.36(-03)	1.88(+13)	2.32(+00)
4.49(-05)	3.98(-02)	4381	3.25(-03)	3.77(+13)	1.77(+00)
5.47(-05)	6.60(-02)	4237	5.05(-03)	7.02(+13)	1.32(+00)
8.30(-05)	1.09(-01)	4093	8.01(-03)	1.26(+14)	9.53(-01)
1.63(-04)	1.81(-01)	3949	1.18(-02)	2.25(+14)	6.71(-01)
3.74(-04)	3.02(-01)	3805	1.57(-02)	4.10(+14)	4.61(-01)
6.77(-04)	4.27(-01)	3835	2.15(-02)	5.76(+14)	5.03(-01)
1.51(-03)	6.77(-01)	3890	3.35(-02)	9.03(+14)	5.88(-01)
4.17(-03)	1.20(+00)	3970	5.90(-02)	1.57(+15)	7.10(-01)
1.16(-02)	2.14(+00)	4040	1.02(-01)	2.75(+15)	8.28(-01)
2.65(-02)	3.38(+00)	4105	1.59(-01)	4.30(+15)	9.45(-01)
6.04(-02)	5.37(+00)	4175	2.50(-01)	6.72(+15)	1.00(+00)
1.15(-01)	7.70(+00)	4225	3.52(-01)	9.53(+15)	1.00(+00)
2.29(-01)	1.12(+01)	4382	5.80(-01)	1.34(+16)	1.01(+00)

TABLE 7

SUMMARY OF RESULTS*

Star	T_{eff}(K)	log g	T_{min}(K)	T_{min}/T_{eff}	log m (T_{min})	log m_o	log P_o
α CMi[a] F5 IV-V	6500±150	4.0±0.2	5200±150	0.80±0.04	-1.00	-5.0±0.3	-1.0±0.5
Sun[b] G2 V	5770±10	4.44	4450±130	0.77±0.025	-1.50	-5.25±0.2	-0.81±0.2
α Cen A[c] G2 V	5735±110	4.26±0.05	4485±150	0.782±0.04	-2.0	-5.3±0.4	-1.04±0.45
α Cen B[c] K1 V	5225±200	4.48±0.06	3725±200	0.713±0.063	-1.25	-5.5±0.3	-1.02±0.36
α Aur[d] G5 III+	5280±200	2.62±0.2	4700±150	0.89±0.06	+0.0	-4.25±0.35	-1.6±0.5
β Gem[d] K0 III	4830±150	2.9±0.2	3805±100	0.788±0.044	-0.52	-4.8±0.3	-1.9±0.5
α Boo[e] K2 III	4250±100	1.7±0.2	3150±100	0.74±0.04	+0.25	-4.5±0.3	-2.8±0.5
α Tau[d] K5 III	3800±200	1.4±0.2	2700±100	0.71±0.06	-0.52	-3.85±0.3	-2.45±0.5

*all units cgs

[a]Ayres (1975)

[b]Ayres and Linsky (1976)

[c]Paper V

[d]this paper

[e]Paper III

There is disagreement between the Mg II line profiles and our calculations concerning the wavelengths of h_1 and k_1, especially α Tau k_1. This could be due to the low count levels and resulting poor statistics at h_1 and k_1. Since the flux ratios h_2/h_1 and k_2/k_1 are large in all cases, however, the resulting additional uncertainty in the integrated emission fluxes is generally less than $\pm 5\%$ and of no significance.

There also appears to be a systematic difference between the observed Mg II k/h emission flux ratio and the calculations, as seen in Table 4. Uncertainties in the wavelength of h_1 and k_1 have only a small random effect and cannot be the cause; k/h would be too large if the zero level of the observations is systematically high. However, lowering the zero level until $k/h \approx 1.2$ would require an unreasonably large adjustment (see Kondo, Morgan, and Modisette 1975). The k/h ratio could be larger than computed, owing to effectively thin emission ($k/h = 2$) above the limb. Linsky and Avrett (1970) found that Ca II K/H increases with height above the solar limb, and the same should be true for Mg II k/h. Such an extended-atmosphere effect should be largest in α Tau, the most extended atmosphere, but the opposite appears to be true. However, contributions from above the limb owing to inhomogeneities like spicules could produce the observed effect without requiring an obvious correlation with gravity. The ratio k/h would be increased from 1.2 to 1.4 if only 25% of the total emission were effectively thin from above the limb, and this uncertainty corresponds to only about a ± 0.2 dex uncertainty in m_0.

Errors in our photosphere models result from uncertainties in four parameters in addition to the data. Our assumed calcium abundance has a stated uncertainty of $\pm 17\%$ and $\gamma_{\rm VW}(\rm K) = (1.7 \pm 0.5) \times 10^{-8}$ cm^3 rad s^{-1} (Ayres 1977), while our adopted magnesium abundance has a stated uncertainty of $\pm 15\%$ and $\gamma_{\rm VW}(h, k) = (1.0 \pm 0.5) \times 10^{-8}$ cm^3 rad s^{-1} (Ayres and Linsky 1976).

Considering the above uncertainties, we estimate our photospheric temperatures to be accurate to ± 100 K. Uncertainties in the Ca II and Mg II line fluxes translate into uncertainties in the chromospheric $T(m)$ distributions. As noted above, the K line is formed mainly below and the Mg II line mainly above the "hinge" point. Thus $\pm 30\%$ uncertainty in the K line flux corresponds for our models to about a ± 200 K $T_{\rm hinge}$ or a ± 0.2 dex change in log $m_{\rm hinge}$. A $\pm 40\%$ uncertainty in the h and k line fluxes corresponds to a ± 0.35 dex change in log m_0.

ii) *Surface Gravities and the* RE *Models*

Our estimated uncertainties of 0.2 dex in the gravities do not significantly affect our proposed upper photospheres, as discussed in Paper III. However, these uncertainties do lead to an uncertainty in the chromospheric mass scale as $P = mg$. Since the Ca II and Mg II resonance lines are collision-dominated, their emission cores are pressure-sensitive. Hence, for example, our determinations of m_0 are uncertain by ± 0.2 dex owing to the gravity uncertainties alone.

There are potential problems in the computation of theoretical model atmospheres. First, the cooling effect of line blanketing is large, amounting to ~ 500 K at small optical depths in the Sun, and schemes for incorporating line blanketing have improved greatly (Gustafsson *et al.* 1975; Johnson and Krupp 1976; Kurucz 1974; Peytremann 1974), but these methods all assume pure absorption which overestimates the surface cooling. Second, there may be important molecular sources still missing in the OS and ODF line-blanketing programs. Third, the theory of convection is crude and the physical picture of convection near the surface of cool stars may be quite inaccurate (cf. Cloutman 1976). Finally, atmospheric inhomogeneities tend to distort the spectrum, especially in the blue, in the sense of producing greater emission in the K line wings than would a true average temperature distribution. Thus estimates of the amount of photospheric nonradiative heating based on the difference between semiempirical and RE models must be regarded as quite uncertain.

iii) *Circumstellar Envelope in α Tauri*

The Aldebaran K line profiles in Figure 1 are asymmetric in the sense of a strong $K_{2\,\rm red}$ emission peak and a narrow absorption feature where one would expect to see the $K_{2\,\rm blue}$ emission peak. Linsky and Worden (1976) and Vaughan and Skumanich (1970) have seen similar K line asymmetries which they attribute to a stellar wind or circumstellar (CS) envelope. The α Tau h and k emission cores (Kondo, Morgan, and Modisette 1975; McClintock *et al.* 1975) also appear asymmetric at 0.4 Å resolution with the red emission peaks much brighter than the blue peaks and the central minimum shifted to the blue. McClintock *et al.* (1978) have analyzed high-resolution *Copernicus* observations of the Arcturus k line, which has the same shape, and have shown that this line shape cannot be due to interstellar absorption but is, rather, intrinsic to the star.

Reimers (1977) has noted that late K luminosity class III giants lie on the edge of the domain of stars with CS envelopes. These stars, of which Aldebaran is a well-known example, have weak CS components in the K line which are variable in velocity and strength, and even disappear occasionally. We have obtained good-quality Aldebaran K and H line profiles on six occasions during 1976. These data are presented in Figures 2 and 3, and the circumstances of observation are listed in Table 2.

In general, we establish wavelength scales by observing a thorium lamp before or after each set of observations and correcting for the stellar radial velocity and terrestrial heliocentric motions. This was done for the 1976 October 29 K line profile, but was not feasible for several of the other K line profiles in Figure 2. We therefore shifted these profiles in wavelength so as to force coalignment of the 3930.5 Å photospheric line (the deep line near the left edge of the figure) with this line in the 1976 October 29 profile.

Each K line profile shows a CS absorption feature at -21 to -33 km s^{-1}, as given in Table 2. Additional absorption features may be present, including features at $+1$ and $+4$ km s^{-1} in the 1976 February 28 profile and weaker CS features adjacent to the major CS features in the 1976 October 29, October 27, and February 26 profiles. These data exhibit evidence for minor changes in the CS absorption on a time scale of 2–3 days and a major change in velocity by 10 km s^{-1} on a time scale of seven months. These time scales have been previously noted by Reimers (1977). In addition, Liller (1968) has noted that the α Tau $K_{2\,red}/K_{2\,blue}$ ratio varies on a time scale of hours and the emission itself varies by up to 20%, and Bohannan (1977) noticed similar variations in the $K_{2\,red}/K_{2\,blue}$ ratio on a time scale of less than 1 hour.

The H line profiles in Figure 3 differ somewhat from the K line profiles taken at about the same time because chromospheric H_2 emission peaks occur closer to line center and there is weaker CS absorption. These result directly or indirectly from the Ca II H line's being a factor of 2 less opaque than the K line. The H_2 peaks probably occur closer to line center as a result of the increase in nonthermal velocities with height, and the CS H line is much weaker than K, as both lines may be on the linear part of the curve of growth. In any case, these effects act together in uncovering the H_2 blue emission, whereas the K_2 blue emission is typically masked by overlying CS absorption.

Vaughan and Skumanich (1970) have estimated equivalent widths for K line CS absorption in α Tau and other stars by assuming that the intrinsic chromospheric line profile is symmetric about line center. In practice they obtain an equivalent width for CS absorption by ratioing the observed emission blueward of line center to the red emission peak reflected about line center. Their assumption is valid only if there are no systematic velocity fields (cf. Chiu *et al.* 1977), and is probably invalid for α Tau. We say this because the H line profiles in Figure 3 have $H_{2\,blue}$ emission peaks which appear to be unaffected by CS absorption and are considerably weaker than the $H_{2\,red}$ peaks. We therefore feel that the most accurate way to estimate Ca II CS column densities for α Tau is to derive CS H line rather than K line equivalent widths. This we do by estimating intrinsic chromospheric $H_{2\,blue}$ emission features (see Fig. 3) and taking the ratios of the observed profiles in this region to the estimated intrinsic profiles.

The inset in Figure 3 shows the CS line profiles obtained in this manner. The FWHM are 150 and 103 mÅ for the 1976 October 29 and September 17 profiles, respectively, considerably larger than the instrumental width of 55 mÅ. Owing to the width and shallowness of these lines, it is reasonable to assume that they are on the linear part of the curve of growth. The measured equivalent widths and derived Ca II column densities are given in Table 2. We note that, if Ca II is the predominant ionization stage for calcium and if the Ca/H abundance ratio is 2.40×10^{-6}, then the hydrogen column density $N_H = 1.4 \times 10^{17}$ cm^{-2}, about 1×10^{-5} that of α Ori (Bernat 1977).

Despite K line profile variations, the position and flux at K_1 is apparently constant, so that our determination of the structure near T_{min} is not seriously affected. Also, a variation in emission flux of up to 20% is only as large as our calibration uncertainty and would not significantly affect our lower chromosphere models (see Table 4). Similarly, any reduction of the *h* and *k* emission fluxes by an absorption feature would most likely be within the Mg II calibration uncertainty.

b) *Comparison with the Haisch-Linsky Transition Region and Mullan Corona for Capella*

Haisch and Linsky (1976) (hereafter HL) estimated a transition-region (TR) pressure $P_{TR} = 1.5$ dyn cm^{-2}, corresponding to $m(TR) = 4 \times 10^{-3}$ g cm^{-2}, for the α Aur primary. HL used rocket observations (Vitz *et al.* 1976) of ultraviolet emission lines of Si II, C II, Si III, C III, Si IV, and N V and *Copernicus* observations (Dupree 1975) of O VI. Their analysis was based on an assumed energy equation in which the divergence of the downward conductive flux from the corona is balanced by radiative losses in the TR. The computed TR is geometrically narrow, as in the Sun, and considerably less than one pressure-scale height, and consequently P_{TR} is a constant. In the present analysis we find $\log m_0 = -4.25 \pm 0.35$ for the α Aur primary after correcting for the flux of the secondary, assuming the same gravity and chemical composition and virtually the same angular diameter as HL. Also, since the Vitz *et al.* data were fortuitously obtained on the same day as the present Mg II data, one cannot ascribe the apparent inconsistency to differing plage activity.

The fundamental problem is that assuming hydrostatic equilibrium, P_{TR} must be less than or equal to P_0, as the transition region lies above the chromosphere. We have, however, derived in the present paper $P_0 = 0.022$ dyn cm^{-2} compared with the HL value of $P_{TR} = 1.5$ dyn cm^{-2}, a significant discrepancy. One possible resolution of this discrepancy could be the inclusion of important terms ignored in the HL energy equation. HL predict, and Dupree's (1975) observations confirm, a wind speed of 0.2 times the local sound speed where the O VI lines are formed ($T \approx 300{,}000$ K). Assuming a time-independent temperature structure, this flow constitutes an additional loss term in the energy balance equation. Also, dissipation of acoustic energy in such a flow could be an additional heating term. In any case, if the temperature structure is not determined by thermal conduction, then the TR need not be thin and the observed line fluxes could be produced by long path lengths and TR pressures possibly as low as $P_0 = 0.022$ dyn cm^{-2}.

Mullan (1976) has predicted a coronal base pressure $P_{CB} = 0.016$ dyn cm^{-2} and temperature $T_c = 530{,}000$ K for the Capella primary on the assumption that the fraction ϕ of the stellar luminosity used to heat the corona is the same as for the Sun, ϕ_S. There is no physical basis for this assumption, and assuming $\phi = \phi_S$, he is unable to compute coronal models for

giants any cooler than β Gem owing to the large heating rates. However, within the uncertainty of our analysis, we are in agreement.

c) *Trends in T_{min}/T_{eff} and m_0*

Eight stars have now been analyzed in this stellar model chromospheres series: four on or near the main sequence ($\log g \geq 4.0$) and four giants. Two principal trends appear in the data presented in Table 7 and Figure 7.

Figure 7*a* is a plot of T_{min}/T_{eff} versus T_{eff} for all eight stars. T_{min}/T_{eff} appears to decrease with decreasing T_{eff} and there may be a separate relation for main-sequence stars and giants. The basic trend can be understood in terms of the effects of CO cooling as described by Johnson (1973), who found that the CO cooling is most effective in the outer layers of his models for 5000 K $\leq T_{eff} \leq$ 4000 K and is most important in low-gravity stars. We find an apparent contradiction to this gravity effect, as T_{min}/T_{eff} for the dwarf star α Cen B is cooler than that for the giants β Gem, α Aur, and α Boo. There are two plausible explanations for the relatively cool T_{min} of α Cen B—the star may be metal-rich (Paper V), which would increase line blanketing; and the importance of scattering in the lines rather than pure absorption assumed by Johnson should increase with decreasing gravity so that the giants have less surface cooling than the dwarfs.

Figure 7*b* is a plot of $\log m_0$ versus T_{eff} for all eight stars which suggests a trend of $\log m_0$ with T_{eff} sloping

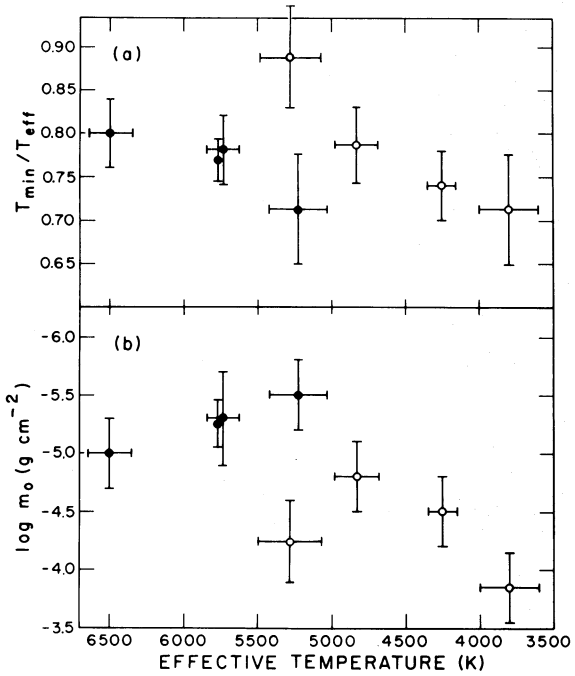

FIG. 7.—(*a*) T_{min}/T_{eff} versus T_{eff} for all eight stars. Data and error bars as in Table 5. *Filled circles*, dwarf group; *open circles*, giants. (*b*) $\log m_0$ versus T_{eff}. Notations same as in Fig. 7*a*.

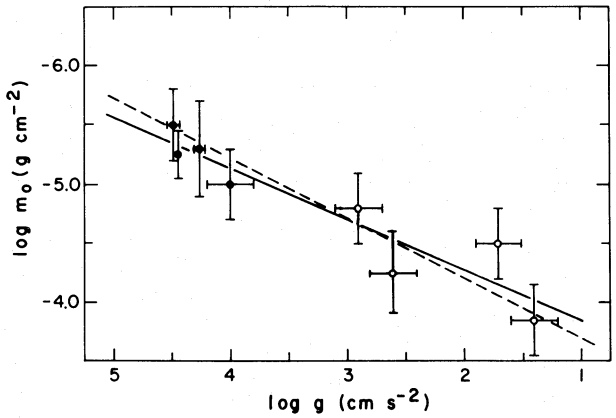

FIG. 8.—$\log m_0$ versus $\log g$. Notations same as in Fig. 7*a*. *Solid line*, least-squares fit to data points (excluding the α Aur value at $\log m_0 \leq -6.0$). *Dashed line*, least-squares fit with imposed slope of -0.5 (excluding the same point).

one way for the giants and the other way for the dwarfs. These trends may be spurious, however, as $\log m_0$ correlates with $\log g$ well for *all* stars as shown in Figure 8, and this correlation has a physical explanation. The solid line represents a least-squares fit to the data. The slope of the curve is -0.43.

We can derive a scaling law between m_0 and g based on the definition of m_0 as the mass point at which $\tau \approx 1.0$ at the head of the Lyman continuum. Since the opacity at this point is due mainly to hydrogen photoionization, $\kappa \sim n_H$, the neutral hydrogen number density, which is in turn proportional to $P/T = mg/T$. This results in $\kappa \sim mg/T$. If we assume that T is constant, then integrating $d\tau = \kappa dm$ yields $\tau \sim m^2 g$. Therefore, at $\tau = 1$, $m_0 \sim g^{-0.5}$ and $P_0 = m_0 g \sim g^{+0.5}$. A least-squares fit to the data constrained to have the slope $d \log m_0 / d \log g = -0.5$, is given by the dashed line in Figure 8. The theoretical and empirical lines agree remarkably well, considering the simplicity of our proposed scaling law, but it is possible to produce better agreement. In the region of m_0, the local temperature rises steeply toward smaller m. If we assume an approximate functional relationship $T(m) = T_0(m/m_0)^{-n}$, then $m_0 \sim g^{-(1/n+2)}$. To match the observed slope of -0.43, we find $n = 0.33$. This argument should not be considered a reliable derivation of $T(m)$ near m_0, but rather an attempt to show the consistency of our $m_0 \sim g^{-(1/n+2)}$ relation.

Physically, this relation can be understood as a result of hydrogen's ionizing at greater mass column densities with decreasing gravity, and thus density. This correlation is similar to that derived by Ayres, Linsky, and Shine (1975) relating $m(T_{min})$ to gravity through the P^2 dependence of H^- opacity.

VII. CONCLUSIONS

This analysis of G and K giants together with our previous studies of stellar and solar chromospheres suggests certain conclusions.

1. It is feasible to derive detailed models of the chromospheres and upper photospheres of late-type

dwarfs and giants based on PRD analyses of the Ca II K line profiles and Mg II *h* and *k* line fluxes, provided that one has absolute fluxes and can estimate the stellar gravity and angular diameter. These models do not assume RE, but they are no better than the assumptions of plane-parallel geometry, hydrostatic equilibrium, and one-dimensional atmospheres. These latter three assumptions are not easily tested. Consequently, we present tabulated models for β Gem and α Tau in the hope that these models will be tested by comparison of computed and observed line profiles and continua. In particular, our inability to match the observed k/h flux ratios suggests considerable emission off-limb, possibly by stellar spicules.

2. As previously found for dwarfs including the Sun, the upper photosphere temperature distributions for late-type giants are hotter than the predictions of RE models which include LTE line blanketing computed by various statistical schemes. This discrepancy could be due to the pure absorption treatment of line blanketing, to considerable temperature inhomogeneities in the stellar photospheres (see Heasley *et al.* 1976), or to photospheric radiative damping of acoustic or other wave modes generated in the convective zone. The major cause of the discrepancy is unclear even for the Sun.

3. The eight stars now studied show an apparent trend of decreasing $T_{\rm min}/T_{\rm eff}$ with decreasing $T_{\rm eff}$. CO line blanketing may be an important cause of this trend.

4. There is a clear trend of decreasing $\log m_0$ with decreasing gravity, which is explicable by hydrogen ionization's occurring at larger mass column densities in lower-gravity stars which have lower-density chromospheres. This scaling law, together with the usual result that $T_0 = 8000$ K, the $m(T_{\rm min})$-gravity scaling law of Ayres, Linsky, and Shine (1975), and our correlations of $T_{\rm min}/T_{\rm eff}$ with $T_{\rm eff}$, specifies the lower and upper boundary condition on $T(m)$ in a chromosphere. It is therefore now feasible to predict *a priori* temperature structures and thus models for quiet chromosphere stars. The validity of this rash statement must be ascertained by deriving semiempirical models for classes of stars not yet studied, including supergiants and hot and cool dwarfs.

5. We derive $P_0 = 0.022$ dyn cm^{-2} for α Aur, which is inconsistent with the Haisch and Linsky transition region pressure $P_{\rm TR} = 1.5$ dyn cm^{-2} on hydrostatic equilibrium grounds. We suggest that, if additional terms are added to the TR energy equation assumed by HL, then $P_{\rm TR}$ could be reduced to be consistent with our value of P_0.

6. We provide additional evidence for a variable circumstellar envelope in α Tau. We feel that the H line is best suited for deriving Ca II circumstellar column densities in this star, as the $H_{2\,\rm blue}$ emission peak is almost completely uncovered in our data. Using the H line data, we derive Ca II column densities of 3.1–3.7 $\times 10^{11}$ cm^{-2}, implying a CS hydrogen column density about 1×10^{-5} that of α Ori.

We thank Robert Kurucz for computing radiative equilibrium models and proofreading the manuscript and Bernhard Haisch, William McClintock, and William Bidelmann for discussions. We gratefully acknowledge support of the National Aeronautics and Space Administration under grants NGL-06-003-057 and NAS5-23274 to the University of Colorado and NGR-4-001-001 to the Johns Hopkins University.

REFERENCES

Athay, R. C., and Lites, B. W. 1972, *Ap. J.*, **176**, 809.
Ayres, T. R. 1975, Ph.D. thesis, University of Colorado.
———. 1977, *Ap. J.*, **213**, 296.
Ayres, T. R., and Johnson, H. R. 1977, *Ap. J.*, **214**, 410.
Ayres, T. R., and Linsky, J. L. 1975, *Ap. J.*, **200**, 660 (Paper III).
———. 1976, *Ap. J.*, **205**, 874.
Ayres, T. R., Linsky, J. L., Rodgers, A. W., and Kurucz, R. L. 1976, *Ap. J.*, **210**, 199 (Paper V).
Ayres, T. R., Linsky, J. L., and Shine, R. A. 1974, *Ap. J.*, **192**, 93 (Paper II).
———. 1975, *Ap. J.* (*Letters*), **195**, L121.
Barnes, T. G., and Evans, D. S. 1976, *M.N.R.A.S.*, **174**, 489.
Bell, R. A., Eriksson, K., Gustafsson, B., and Norlund, A. 1976, *Astr. Ap. Suppl.*, **23**, 37.
Bernat, A. P. 1977, *Ap. J.*, **213**, 756.
Blazit, A., Bonneau, D., Fosse, M., Koechlin, L., Labeyrie, A., and Oneto, F. L. 1977, *Ap. J.* (*Letters*), **217**, L55.
Bohannan, B. 1977, private communication.
Chiu, H.-Y. 1977, *Appl. Optics*, **16**, 237.
Chiu, H.-Y., Adams, P. S., Linsky, J. L., Basri, G. S., Maran, S. P., and Hobbs, R. W. 1977, *Ap. J.*, **211**, 453.
Cloutman, L. 1976, *Bull. AAS*, **8**, 533.
Conti, P. S., Greenstein, J. L., Spinrad, H., Wallerstein, G., and Vardya, M. S. 1967, *Ap. J.*, **148**, 105.
Currie, D. G., Knapp, S. L., and Liewer, K. M. 1974, *Ap. J.*, **187**, 131.
Dupree, A. K. 1975, *Ap. J.* (*Letters*), **200**, L27.
de Jager, C., Kondo, Y., van der Hucht, K. A., and Morgan, T. H. 1976, 19th Meeting, COSPAR, Philadelphia (1976 June 14–19).
Gliese, W. 1969, *Veröff. Astr. Rechen-Inst. Heidleberg*, No. 22.
Gustafsson, B., Bell, R. A., Eriksson, K., and Norlund, Å. 1975, *Astr. Ap.*, **42**, 407.
Gustafsson, B., Kjaergaard, P., and Andersen, S. 1974, *Astr. Ap.*, **34**, 99.
Haisch, B. M., and Linsky, J. L. 1976, *Ap. J.* (*Letters*), **205**, L39 (HL).
Heasley, J. N., Ridgway, S. T., Carbon, D. F., Milkey, R. W., and Hall, D. N. B. 1976, *Bull. AAS*, **9**, 324.
Herbig, G. H., and Spalding, J. F. 1955, *Ap. J.*, **121**, 118.
Honeycutt, R. K., Ramsey, L. W., Warren, W. H., and Ridgeway, S. T. 1977, *Ap. J.*, **215**, 584.
Iben, I. 1967, *Ann. Rev. Astr. Ap.*, **5**, 571.
Johnson, H. L. 1966, *Ann. Rev. Astr. Ap.*, **4**, 193.
———. 1967, *Comm. Lunar Planet. Lab.*, **6**, 85.
Johnson, H. L., Mitchell, R. I., Iriarte, B., and Wisnewski, W. Z. 1966, *Comm. Lunar Planet. Lab.*, **4**, 99.
Johnson, H. R. 1973, *Ap. J.*, **180**, 81.
Johnson, H. R., and Krupp, B. 1976, *Ap. J.*, **206**, 201.
Kelch, W. L., Linsky, J. L., Basri, G. S., Chiu, H.-Y., Maran, S. P., and Furenlid, I. 1976, *Bull. AAS*, **8**, 518.
Kondo, Y., Morgan, T. H., and Modisette, J. L. 1975, *Ap. J.* (*Letters*), **196**, L125.
———. 1976, *Ap. J.*, **207**, 167.
Kurucz, R. L. 1974, Dudley Obs. Rept., No. 9.
———. 1977, private communication.
Liller, W. 1968, *Ap. J.*, **151**, 589.
Linsky, J. L., and Avrett, E. H. 1970, *Pub. A.S.P.*, **82**, 169.
Linsky, J. L., and Ayres, T. R. 1978, *Ap. J.*, **220**, 619 (Paper VI).
Linsky, J. L., and Worden, S. P. 1976, *Bull. AAS*, **8**, 519.

McClintock, W. 1977, Ph.D. thesis, The Johns Hopkins University.
McClintock, W., Linsky, J. L., Henry, R. C., Moos, W. H., and Gerola, H. 1975, *Ap. J.*, **202**, 165,
McClintock, W., Moos, H. W., Henry, R. C., Linsky, J. L., and Barker, E. S. 1978, *Ap. J. Suppl.*, **37**, in press.
Milkey, R. W., and Mihalas, D. 1973, *Ap. J.*, **185**, 709.
Milkey, R. W., Shine, R. A., and Mihalas, D. 1975, *Ap. J.*, **199**, 718.
Morgan, W. W., Keenan, P. C., and Kellmann, E. 1943, in *An Atlas of Stellar Spectra* (Chicago: University of Chicago Press), p. 31.
Mount, G. H., and Linsky, J. L. 1975, *Ap. J.* (*Letters*), **202**, L51.
Mullan, D. J. 1976, *Ap. J.*, **209**, 171.
Owocki, S. 1977, private communication.
Paczyński, B. J. 1970, *Acta Astr.*, **20**, 47.
Pease, F. G. 1931, *Ergebn. exacten Naturwiss.*, **10**, 84.
Peytremann, E. 1974, *Astr. Ap.*, **33**, 203.
Ramsey, L. 1977*a*, *Ap. J.*, **215**, 603.
———. 1977*b*, *Ap. J.*, **215**, 827.
Reimers, D. 1977, *Astr. Ap.*, **57**, 395.
Ross, J. E., and Aller, L. H. 1976, *Science*, **191**, 1223.
Shine, R. A. 1973, Ph.D. thesis, University of Colorado.
———. 1975, *Ap. J.*, **202**, 543.
Shine, R. A., and Linsky, J. L. 1974, *Solar Phys.*, **39**, 49.
Stencel, R. E. 1977, *Ap. J.*, **215**, 176.
Tomkin, J., and Lambert, D. L. 1974, *Ap. J.*, **193**, 631.
van Paradijs, J., and Meurs, E. J. A. 1974, *Astr. Ap.*, **35**, 225.
Vaughan, A. H., Jr., and Skumanich, A. 1970, in *Spectrum Formation in Stars with Steady-State Extended Atmospheres*, ed. H. G. Groth and P. Wellmann (NBS Special Pub. No. 332), p. 295.
Vitz, R. C., Weiser, H., Moos, H. W., Weinstein, A., and Warden, E. 1976, *Ap. J.* (*Letters*), **205**, L35.
Wright, K. O. 1954, *Pub. Dom. Ap. Obs.*, **10**, 1.

GIBOR S. BASRI, WALTER L. KELCH, and JEFFREY L. LINSKY: JILA, University of Colorado, Boulder, CO 80309

SHENG-HUEI CHANG: Department of Physics, City College of the City University of New York, New York, NY 10031

HONG-YEE CHIU: Institute for Space Studies, 2880 Broadway, New York, NY 10025

INGEMAR FURENLID: Kitt Peak National Observatory, P.O. Box 26732, Tucson, AZ 85726

STEPHEN P. MARAN: NASA Goddard Space Flight Center, Greenbelt, MD 20771